Ramakrishna Mission Residential College (Autonomous)
Kolkata 700103, WB, India

Collaborative research in coordination chemistry of organic radicals

Number 8

Institute 1: Ramakrishna Mission Residential College (Autonomous)

Concerned Faculty: Dr. Prasanta Ghosh, Dept of Chemistry

&

Institute 2: **Max-Planck-Institut für Chemische Energiekonversion**

Stiftstrasse 34 - 36 / D - 45470 Mülheim an der Ruhr

Concerned Scientist: Dr Thomas Weyhermüller

Period of Investigation: 28-11-2015 to 29-05-2016

Project: Mixed-Valence Anion Radical Complexes of Cobalt: Valence Tautomerism

Output: The result was published in a journal of international repute

Mixed-Valence o-Iminobenzoquinone and o-Iminobenzosemiquinonate Anion Radical Complexes of Cobalt: Valence Tautomerism

Suvendu Maity, Suman Kundu, Sachinath Bera, Thomas Weyhermüller and Prasanta Ghosh*

Eur. J. Inorg. Chem., 2016, *22*, 3680-3690

Dr. Prasanta Ghosh

Dr Thomas Weyhermüller

ChemPubSoc Europe

DOI: 10.1002/ejic.201600525

EurJIC European Journal of Inorganic Chemistry

Full Paper

Anion Radical Complexes

Mixed-Valence *o*-Iminobenzoquinone and *o*-Iminobenzosemiquinonate Anion Radical Complexes of Cobalt: Valence Tautomerism

Suvendu Maity,[a] Suman Kundu,[a] Sachinath Bera,[a] Thomas Weyhermüller,[b] and Prasanta Ghosh*[a]

Abstract: 2,4-Di-*tert*-butyl-*N*-[2-(phenylthio)]phenyl-*o*-iminobenzosemiquinonate anion radical ($L^{SPh}_{ISQ}{}^{\bullet-}$) and *o*-iminobenzoquinone (L^{SPh}_{IQ}) based mixed-valence complexes of the types *trans*-$[Co^{II}(L^{SPh}_{ISQ}{}^{\bullet-})(L^{SPh}_{IQ})X]$ defined by Robin–Day Class III states, *trans*-$[Co^{II}(L^{SPh}_{ISQ}{}^{0.5\bullet-})_2X]$ {X = Cl^-, **1**; SCN^- (thiocyanato-*kS*), **2**; N_3^-, **3**; NO_2^-, **4** and I_3^-, **5**} are reported. The X-ray bond parameters of **1–5**, BS DFT calculations and variable-temperature X-band EPR spectra established the electronic states of **1–5**. It was confirmed that **1–5** and mixed-valence ions $[\mathbf{1–5}]^+$ and $[\mathbf{1–5}]^-$ exhibit valence tautomeric equilibria of types: **1–5**: *trans*-$[Co^{II}(L^{SPh}_{ISQ}{}^{0.5\bullet-})_2X] \rightleftharpoons$ *trans*-$[Co^{III}(L^{SPh}_{ISQ}{}^{\bullet-})_2X]$; $[\mathbf{1–5}]^+$: *trans*-$[Co^{III}(L^{SPh}_{ISQ}{}^{0.5\bullet-})_2X]^+ \rightleftharpoons$ *trans*-$[Co^{II}(L^{SPh}_{IQ})_2X]^+$, and $[\mathbf{1–5}]^-$: *trans*-$[Co^{III}(L^{SPh}_{ISQ}{}^{0.5\bullet-1.0-})_2X]^- \rightleftharpoons$ *trans*-$[Co^{II}(L^{SPh}_{ISQ}{}^{\bullet-})_2X]^-$ (L^{SPh}_{IQ} = *o*-iminobenzoquinone state of $L^{SPh}_{ISQ}{}^{\bullet-}$). In solids and frozen glasses, the contributions of "$[M^{II}(L^{SPh}_{IQ})]$" states are larger, whereas in fluid solutions the contributions of the "$[M^{III}(L^{SPh}_{ISQ}{}^{\bullet-})]$" states dominate. In CH_2Cl_2, **1–5** absorb strongly at ≥ 800 nm due to spin-allowed $L^{SPh}_{ISQ}{}^{\bullet-} \rightarrow L^{SPh}_{ISQ}{}^{\bullet-}$ (charge resonance transfer) transitions, whereas in solids, they exhibit $M^{II} \rightarrow L^{SPh}_{IQ}$ (MLCT) transitions at ≥ 1000 nm.

Introduction

Electronic structures of the redox non-innocent catechol ($L^{OO}H_2$), *o*-aminophenol ($L^{NO}H_2$), and *o*-phenylenediamine ($L^{NN}H_2$) complexes of transition-metal ions are complex.[1] However, the transition-metal complexes of $L^{OO}H_2$, $L^{NO}H_2$, and $L^{NN}H_2$ are significant and, in many cases, they expand the activity of the central metal ion; particularly, ligand-facilitated oxidative addition reaction and catalysis are noteworthy.[2] Transition-metal complexes $L^{OO}H_2$, $L^{NO}H_2$, and $L^{NN}H_2$ exist in three different electronic states, as depicted in Scheme 1, within a relatively small potential range. These features of such redox non-innocent ligands open up the opportunity to build ligand-based mixed-valence complexes of transition-metal ions.[3]

The electronic states of $L^{OO}H_2$, $L^{NO}H_2$, and $L^{NN}H_2$ complexes depend significantly on the transition-metal ions. Pierpont et al. developed the chemistry of $L^{OO}_{SQ}{}^{\bullet-}$ with different redox-active transition-metal ions.[4] The coordination complexes of $L^{NO}_{ISQ}{}^{\bullet-}$ and $L^{NN}_{DISQ}{}^{\bullet-}$ were reported by many groups, and, in this regard, the precise elucidation of the electronic structures of these complexes using the X-ray bond parameters, various spectra, and DFT calculations by Wieghardt and co-workers are noteworthy.[5]

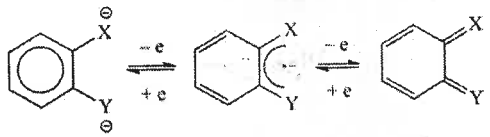

$L^{OO}H_2$	$L^{OO}_{CAT}{}^{2-}$	$L^{OO}_{SQ}{}^{\bullet-}$	L^{OO}_{Q}
$L^{NO}H_2$	$L^{NO}_{AP}{}^{2-}$	$L^{NO}_{ISQ}{}^{\bullet-}$	L^{NO}_{IQ}
$L^{NN}H_2$	$L^{NN}DA^{2-}$	$L^{NN}_{DISQ}{}^{\bullet-}$	L^{NN}_{DIQ}

Scheme 1.

One of the important properties of $L^{OO}_{SQ}{}^{\bullet-}$ is that in complexes, it exhibits valence tautomerism (VT), which is an important phenomenon in chemistry.[4,6] In the vast area of coordination chemistry, VT is particularly limited to *o*-dioxolene complexes of transition-metal ions.[4,7] The existence of valence tautomeric equilibria of types $M^{n+}(L^{OO}_{CAT}{}^{2-}) \leftrightarrow M^{(n-1)+}(L^{OO}_{SQ}{}^{\bullet-})$ and $M^{(n-1)+}(L^{OO}_{SQ}{}^{\bullet-}) \leftrightarrow M^{(n-2)+}(L^{OO}_{Q})$ with different redox-active transition-metal ions was established. Examples of coordination complexes that exhibit valence tautomerism with ligands other than *o*-dioxolene are rare.[8] It is surprising that there is no substantive report of VT on $L^{NO}_{ISQ}{}^{\bullet-}$, except a recent report with iron(III/II) ions.[9] In this project, we confirm the existence of valence tautomeric equilibria of types $M^{n+}(L^{NO}_{ISQ}{}^{\bullet-}) \leftrightarrow M^{(n-1)+}(L^{NO}_{IQ})$ both in the solid state and in solution of a family of $L^{NO}_{ISQ}{}^{\bullet-}$ complexes of cobalt.

The precise metrical parameters and the spectral features of $L^{NO}_{ISQ}{}^{\bullet-}$ and the one-electron reduced and oxidized redox states, $L^{NO}_{AP}{}^{2-}$ and L^{NO}_{IQ}, coordinated to transition-metal ions

[a] Department of Chemistry, R. K. Mission Residential College, Narendrapur, Kolkata-103, India
E-mail: ghosh@pghosh.in
www.pghosh.in
[b] Max-Planck-Institut für Chemische Energiekonversion, Stiftstrasse 34–36, 45470 Mülheim an der Ruhr, Germany

Supporting information for this article is available on the WWW under http://dx.doi.org/10.1002/ejic.201600525.

have been documented (Scheme 1).[1f,1g,5] In this project, the coordination chemistry of 2,4-di-*tert*-butyl-6-{[2-(phenylthio)-phenyl]amino} phenol ($L^{SPh}H_2$), which is a tridentate *o*-aminophenol derivative, was explored. The deprotonated and the oxidized states of the $L^{SPh}H_2$ ligand as 2,4-di-*tert*-butyl-*N*-[2-(phenylthio)]phenyl-*o*-amidophenolato dianion ($L^{SPh}{}_{AP}{}^{2-}$), 2,4-di-*tert*-butyl-*N*-[2-(phenylthio)]phenyl-*o*-iminobenzosemiquinonate anion radical ($L^{SPh}{}_{ISQ}{}^{\bullet-}$) and the neutral 2,4-di-*tert*-butyl-*N*-[2-(phenylthio)] phenyl-*o*-iminobenzoquinone ($L^{SPh}{}_{IQ}$) are illustrated in Scheme 2. The coordination complexes of $L^{SPh}H_2$ reported in this article are depicted in Scheme 3. Complexes **1–5** were substantiated by analytical data, spectra, single-crystal X-ray structure determinations and by density functional theory (DFT) calculations. The members of the electron transfer series $[\mathbf{1–5}]^z$ (z = 2+, 1+, 1–) were investigated by spectroelectrochemical measurements, EPR spectroscopy, and by DFT calculations.

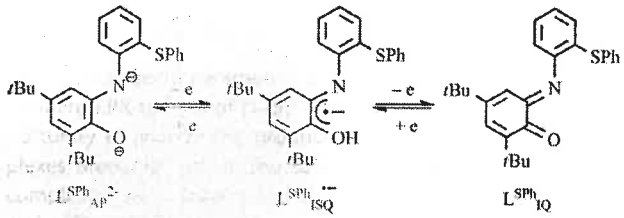

Scheme 2. Redox states of $L^{SPh}{}_{AP}{}^{2-}$ ligand.

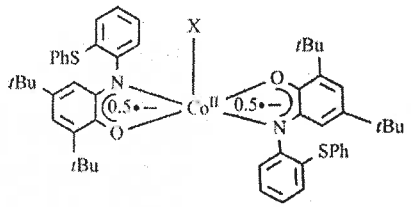

X = Cl^-, **1**; SCN^- (thiocyanato-*k*S) **2**; N_3^-, **3**; NO_2^-, **4**; I_3^-, **5**

Scheme 3. Isolated complexes of cobalt ions.

The X-ray bond parameters of **1–5** and the temperature-dependent EPR spectra of $[\mathbf{1–5}]^+$ and $[\mathbf{1–5}]^-$ ions open up an opportunity to analyze the ground electronic states of the complexes precisely both in the solid and solution state. In these complexes, we substantiated the existence of $L^{SPh}{}_{ISQ}{}^{\bullet-}$, $L^{SPh}{}_{IQ}$, and $L^{SPh}{}_{ISQ}{}^{0.5-}$ states. The average C–O/N lengths, which are more precise parameters (compared with explicit C–O and C–N lengths) to elucidate the electronic states of these delocalized systems, are shorter in comparison to those observed in genuine bis(*o*-iminobenzosemiquinonate) complexes.[10,11] The X-ray bond parameters in conjunction with the DFT calculations predicted a contribution of both $L^{SPh}{}_{ISQ}{}^{\bullet-}$ and $L^{SPh}{}_{IQ}$ states to the ground electronic states of **1–5**, which are defined as ligand-based mixed-valence complexes of types *trans*-$[Co^{II}(L^{SPh}{}_{ISQ}{}^{\bullet-})(L^{SPh}{}_{IQ})X]$. The delocalized states are defined as Robin–Day Class III states[3] of types *trans*-$[Co^{II}(L^{SPh}{}_{ISQ}{}^{0.5-})_2X]$. The investigation revealed that **[1–5]** exhibit different electronic states in solutions and solids because of tautomeric equilibria of types *trans*-$[Co^{II}(L^{SPh}{}_{ISQ}{}^{0.5-})_2X] \rightleftharpoons$ *trans*-$[Co^{III}(L^{SPh}{}_{ISQ}{}^{\bullet-})_2X]$; $[\mathbf{1–5}]^+$ and $[\mathbf{1–5}]^-$ in solutions establish tautomeric equilibria of types $[Co^{III}(L^{SPh}{}_{ISQ}{}^{0.5-})_2X]^+ \rightleftharpoons [Co^{II}(L^{SPh}{}_{IQ})_2X]^+$ and $[Co^{III}(L^{SPh}{}_{ISQ}{}^{0.5-1.0-})_2X]^- \rightleftharpoons [Co^{II}(L^{SPh}{}_{ISQ}{}^{\bullet-})_2X]^-$.

Results and Discussion

Syntheses and Characterization

The cobalt complexes of $L^{SPh}H_2$ isolated in this work are summarized in Scheme 3. The complexes were prepared by the paths depicted in Scheme 4. In the bis($L^{SPh}{}_{ISQ}{}^{\bullet-}$) complexes of cobalt, the N or the O atoms of the two ligands lie *trans* to each other and the complexes are abbreviated as *trans*-$[Co^{II}(L^{SPh}{}_{ISQ}{}^{0.5-})_2X]$. Complexes **1–5** were characterized by elemental analyses, mass spectrometry, ^1H, ^{13}C NMR and IR spectroscopic analyses, and by single-crystal X-ray structure determinations. The elemental analyses and the spectroscopic data are summarized in the experimental section. The symmetric and asymmetric stretching vibrations of the SC≡N bond of **2** appeared at 2101 and 2060 cm^{-1}. The strong absorption band at 1983 cm^{-1} of **3** was assigned to the stretching vibration of the coordinated N_3^- ion. The symmetric and asymmetric stretching vibrations of the NO bonds of the coordinated NO_2 in **5** resonate at 1282 and 1264 cm^{-1}.

$$Co^{II}Cl_2 + 2L^{SPh}H_2 + 3/2\ O_2 \longrightarrow \mathbf{1} + 3/2\ H_2O + HCl$$

$$Co^{II}Cl_2 + 2L^{SPh}H_2 + 3/2\ O_2 + NaSCN \longrightarrow \mathbf{2} + 3/2\ H_2O + HCl + NaCl$$

$$Co^{II}Cl_2 + 2L^{SPh}H_2 + 3/2\ O_2 + NaN_3 \longrightarrow \mathbf{3} + 3/2\ H_2O + HCl + NaCl$$

$$Co^{II}Cl_2 + 2L^{SPh}H_2 + 3/2\ O_2 + NaNO_2 \longrightarrow \mathbf{4} + 3/2\ H_2O + HCl + NaCl$$

$$\mathbf{3} + 3/2I_2 \longrightarrow \mathbf{5} + 3/2N_2$$

Scheme 4. Synthetic reactions of **1–5**.

Assignments of the NMR spectra (^1H and ^{13}C) of these complexes are difficult. However, to support the assignments, ^1H and ^{13}C NMR spectra of $[Co(L^{SPh-tBu})_2Cl]$ (**1′**) were calculated at the B3LYP/DFT level of the theory using singlet state ($L^{SPh-tBu}H_2$ = $L^{SPh}H_2$ ligand without *tert*-butyl substituent). The calculated data are listed in Chart S1 (Supporting Information). It is noted that the hydrogen atoms of the aminophenol rings of complexes **1–5** are shielded in comparison to those of the ligand. ^{13}C NMR spectroscopic data reveal that two carbon atoms bonded to O, N atoms are deshielded more than that of the free ligand. The ^{13}C NMR spectrum of **1** is illustrated Figure S1. In the free ligand, they appear at 149.66 and 148.65 ppm. The experimental ^{13}C NMR signals at 182.0–185.0 and 167.0–168.0 ppm due to these two carbon atoms of **1–5** correspond to those of sp^2 carbon atoms, reflecting the quinoidal distortion of the ring in the complexes.[12]

Assignment of the Electronic States

In conjunction with the X-ray bond parameters and EPR spectroscopy, DFT calculations were employed to elucidate the electronic structures of **1–5** and the members of their electron-

transfer series. The single-crystal X-ray structure determinations of **1–5** confirmed the molecular geometries and the bond parameters of the complexes in the crystalline state. The crystallographic data are summarized in Table S1. The molecular geometries and the atom labeling schemes are illustrated in Figure 1. The X-band EPR spectral parameters of CH_2Cl_2 solutions of [**1–5**]$^+$ and [**1–5**]$^-$ ions are summarized in Table S2. To analyze the bond parameters and atomic spin densities, DFT calculations were performed on $[Co(L^{SPh-tBu})_2Cl]$ (**1′**) and $[Co(L^{SPh-tBu})_2N_3]$ (**3′**); $[Co(L^{SPh-tBu})_2Cl]^+$ (**1′**$^+$), $[Co(L^{SPh-tBu})_2Cl]^-$ (**1′**$^-$), and $[Co(L^{SPh-tBu})_2N_3]^-$ (**3′**$^-$) and the optimized coordinates are listed in Tables S12–17.

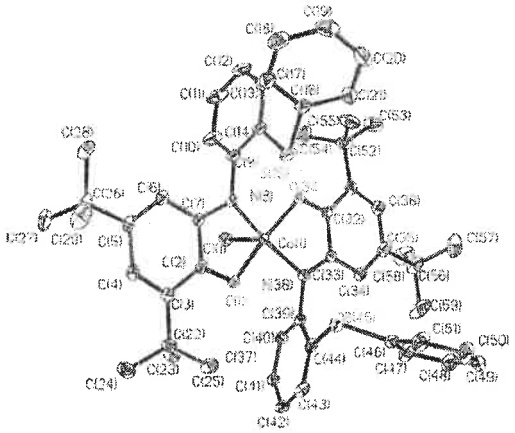

1

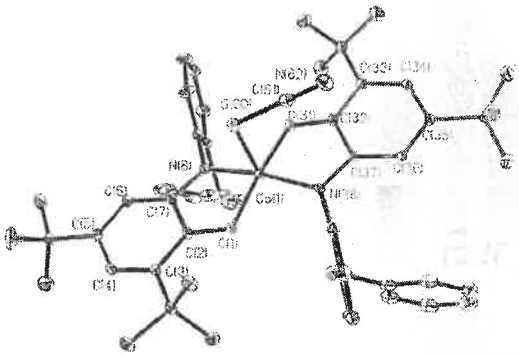

2

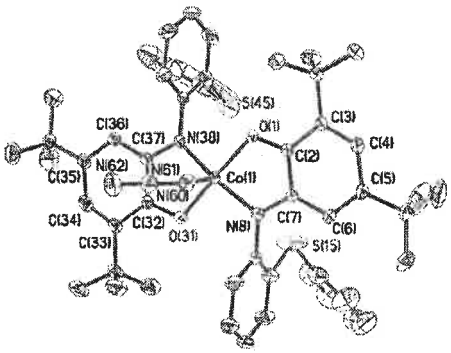

3

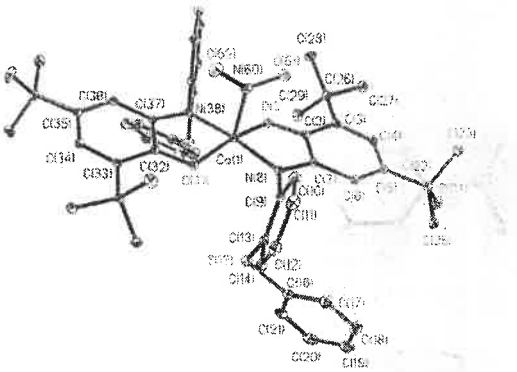

4

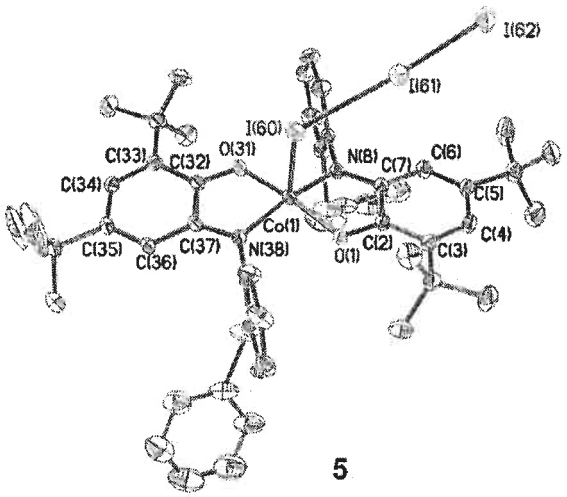

5

Figure 1. Molecular geometries of **1–5** in crystals (40 % thermal ellipsoids, hydrogen atoms and solvent are omitted for clarity).

Mixed-Valence Complexes 1–5, [1–5]$^-$, and [1–5]$^+$

Complexes **1–5** are isostructural and crystallize in $P\bar{1}$, $C2/c$, $P2_1/c$, $P\bar{1}$, and $P2_1/n$ space groups. Selected bond parameters are summarized in Table 1. Complexes **1–5** exhibit square-pyramid geometries with the halide or pseudo halide or nitrite at the apical positions. The bond parameters of the coordination spheres and the ligands of **1–5** are similar (Table 1). The Co–O and Co–N lengths span the ranges of 1.865 ± 0.016 and 1.856 ± 0.009 Å. The average C–O and C–N lengths of the *o*-aminophenol derivatives of **1–5** are as follows: **1**, C–O, 1.292(2) and C–N, 1.337(2); **2**, C–O, 1.297(2) and C–N, 1.345(2); **3**, C–O, 1.297(2) and C–N, 1.347(2); **4**, C–O, 1.299(2) and C–N, 1.344(2); **5**, C–O, 1.294(2) and C–N, 1.335(2) Å. The C–C lengths of the central phenyl rings of the two ligands exhibit quinoidal long–short–long–short–long types of distortions, as indicated in Table 1. The C–O and C–N bond parameters explicitly indicate that both ligands are oxidized.[10,11] In cases of **1–5**, there are two possibilities: either both ligands are oxidized to $L^{SPh}{}_{ISQ}{}^{\bullet-}$, as in *trans*-[$Co^{III}(L^{SPh}{}_{ISQ}{}^{\bullet-})_2X$] ($S_t$ = 0), or one ligand is oxidized to $L^{SPh}{}_{ISQ}{}^{\bullet-}$ and the second is oxidized by two electrons to $L^{SPh}{}_{IQ}$ affording mixed-valence complexes of types *trans*-[$Co^{II}(L^{SPh}{}_{ISQ}{}^{\bullet-})(L^{SPh}{}_{IQ})X$] or the delocalized Robin–Day Class III states of types *trans*-[$Co^{II}(L^{SPh}{}_{ISQ}{}^{0.5\bullet-})_2X$], as depicted in Scheme 5. To distinguish these two states, the average C–O/N lengths of the two equivalent ligands were used. The average C–O/N lengths of the *trans*-[$Co^{III}(L^{SPh}{}_{ISQ}{}^{\bullet-})_2X$] state are expected to be 1.335 ± 0.010 Å, whereas the same for the valence tautomers, *trans*-[$Co^{II}(L^{SPh}{}_{ISQ}{}^{0.5\bullet-})_2X$] are 1.308 ± 0.010 Å, as listed in Table 2.

The average C–O/N lengths of **1–5** obtained from the single-crystal X-ray structure determinations as listed in Table 2, are 1.319 ± 0.004 Å, which are shorter than for $L^{NO}{}_{ISQ}{}^{\bullet-}$. The average C–O/N lengths of $L^{NO}{}_{ISQ}{}^{\bullet-}$ in the complexes, where VT are not expected, are listed in Chart S2. In this context, the C–O/N lengths of [$Co^{III}(L^{NO}{}_{ISQ}{}^{\bullet-})_2NO$] complex are significant.[10a] The C–O and C–N lengths are longer than those of **1–5**. The average C–O/N lengths of [$Co^{III}(L^{NO}{}_{ISQ}{}^{\bullet-})_2NO$] precisely correlate to the bis(*o*-iminpobenzosemiquinonate) state because tautomerization to the [$Co^{II}(L^{NO}{}_{ISQ}{}^{\bullet-})(L_{IQ})NO$] state with [CoNO][9] is not energetically favorable.

The average C–O/N lengths (1.319 ± 0.004 Å) do not unambiguously support the existence of the *trans*-[$Co^{III}(L^{SPh}{}_{ISQ}{}^{\bullet-})_2X$] state in the solids of **1–5**; rather, the bond parameters are consistent with *trans*-[$Co^{II}(L^{SPh}{}_{ISQ}{}^{0.5\bullet-})_2X$] states. The existence of these *trans*-[$Co^{II}(L^{SPh}{}_{ISQ}{}^{0.5\bullet-})_2X$] states in **1–5** was further established by using broken symmetry (BS) DFT calculations (see below).

The bond parameters of the axial ligands are summarized in Table S4. The Co–Cl, Co–SCN, Co–N_3, Co–NO_2, and Co–I_3 lengths are 2.235(2), 2.287(1), 1.982(2), 1.928(2), and 2.602(2) Å, respectively. The chloride ion is a σ-bonding ligand and the Co^{II}–Cl

Table 1. Selected lengths [Å] of **1–5** determined experimentally.

	1 (100 K)	**1** (296 K)	**2** (296 K)	**3** (296 K)	**4** (100 K)	**5** (296 K)
Co(1)–O(1)	1.865(2)	1.883(2)	1.865(2)	1.871(2)	1.850(1)	1.857(3)
Co(1)–N(8)	1.862(2)	1.849(2)	1.856(2)	1.851(2)	1.859(2)	1.864(4)
Co(1)–O(31)	1.848(2)	1.868(2)	1.874(2)	1.882(2)	1.857(1)	1.865(3)
Co(1)–N(38)	1.866(2)	1.858(2)	1.844(2)	1.842(2)	1.855(2)	1.859(4)
O(1)–C(2)	**1.293(2)**	**1.293(3)**	**1.296(2)**	**1.294(3)**	**1.298(2)**	**1.297(6)**
C(2)–C(3)	1.429(2)	1.436(4)	1.435(2)	1.428(3)	1.429 (2)	1.432(7)
C(3)–C(4)	1.373(2)	1.364(5)	1.374(2)	1.371(3)	1.375 (2)	1.378(7)
C(4)–C(5)	1.442(2)	1.444(5)	1.441(2)	1.422(4)	1.439 (2)	1.444(7)
C(5)–C(6)	1.363(2)	1.359(4)	1.368(2)	1.353(3)	1.371(2)	1.351(7)
C(6)–C(7)	1.416(2)	1.412(4)	1.420(2)	1.412(3)	1.422(2)	1.427(6)
C(7)–N(8)	**1.340(2)**	**1.341(3)**	**1.345(2)**	**1.344(3)**	**1.343(2)**	**1.340(6)**
C(2)–C(7)	1.443(2)	1.442(4)	1.440(2)	1.437(3)	1.443(2)	1.435(7)
O(31)–C(32)	**1.292(2)**	**1.298(3)**	**1.298(2)**	**1.300(3)**	**1.302(2)**	**1.291(5)**
C(32)–C(33)	1.429(2)	1.431(4)	1.431(2)	1.431(3)	1.435(2)	1.429(7)
C(33)–C(34)	1.365(2)	1.371(4)	1.376(2)	1.367(4)	1.377(2)	1.373(7)
C(34)–C(35)	1.434(3)	1.435(5)	1.435(2)	1.428(4)	1.437(2)	1.436(8)
C(35)–C(36)	1.366(2)	1.358(4)	1.371(2)	1.356(3)	1.370(2)	1.354(7)
C(36)–C(37)	1.421(2)	1.417(4)	1.414(2)	1.439(3)	1.421(2)	1.431(7)
C(32)–C(37)	1.441(2)	1.438(4)	1.441(2)	1.439(3)	1.438(2)	1.448(7)
C(37)–N(38)	**1.333(2)**	**1.342(4)**	**1.346(2)**	**1.350(3)**	**1.345(2)**	**1.335(6)**

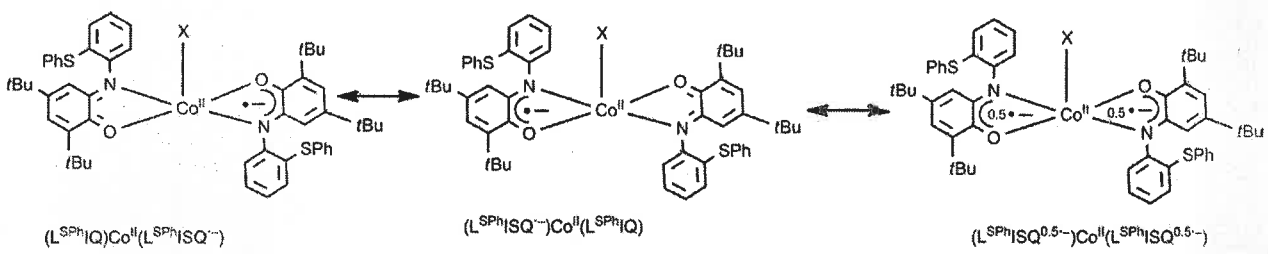

Scheme 5. Electronic states of **1–5**.

Table 2. Expected average C–O/N lengths of bis($L_{ISQ}^{\bullet-}$)Co^{III} and bis($L_{ISQ}^{0.5\bullet-}$)Co^{II} states and experimental average C–O/N lengths of **1–5** at 296 K.

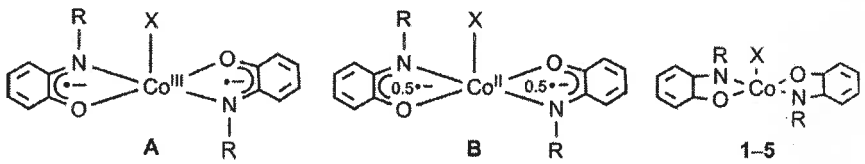

	A	B	1	2	3	4	5
avg C–N	1.360 ± 0.010	1.335 ± 0.010	1.341(3)	1.345(2)	1.347(3)	1.344(2)	1.337(6)
avg C–O	1.310 ± 0.010	1.280 ± 0.010	1.295(3)	1.296(2)	1.297(3)	1.299(2)	1.294(6)
avg C–O/N	1.335 ± 0.010	1.308 ± 0.010	1.318(3)	1.320(2)	1.322(3)	1.322(2)	1.315(6)

and Co^{III}–Cl lengths are significantly different in the complexes.[13] To investigate the effect of temperature on the contributions of [$Co^{II}(L^{SPh}{}_{ISQ}{}^{0.5\bullet-})_2X$] and [$Co^{III}(L^{SPh}{}_{ISQ}{}^{\bullet-})_2X$] components to the crystals of **1–5**, the X-ray structure of **1** was determined at 296 and 100 K. Selected bond parameters are summarized in Table 1. It is observed that the average C–O/N lengths are 1.314(2) Å, which are shorter than those observed at 296 K, inferring a higher contribution of the [$Co^{II}(L^{SPh}{}_{ISQ}{}^{0.5\bullet-})_2Cl$] state to **1** at lower temperature. The higher contribution of cobalt(II) ion is reflected in the longer Co–Cl length (2.251(1) Å) in **1** at 100 K compared with that at 296 K (2.235(2) Å). The data indicates the existence of a thermal equilibrium of *trans*-[$Co^{III}(L^{SPh}{}_{ISQ}{}^{\bullet-})_2X$] and [$Co^{II}(L^{SPh}{}_{ISQ}{}^{0.5\bullet-})_2X$] states in solids of **1–5**.

DFT calculations were performed on *trans*-[$Co(L^{SPh-tBu})_2Cl$] (**1′**) to predict the electronic structures of **1–5**. The gas-phase geometry of **1′** was optimized with the singlet spin state. Similar to **2**, the HOMO and LUMOs of the CSS state of **1′** scatter on cobalt and π orbitals of two ligands. Further analyses established that the CSS solution of **1′** is unstable due to OSS perturbation. Broken symmetry (BS) calculations confirmed that the OSS solution of **1′** is more stable than the CSS solution by 11.2 kJ/mol. The calculated bond parameters of the BS state of **1′**, as summarized in Table S5, are similar to those obtained from the single-crystal X-ray structure determinations of **1–5**. The calculated average C–O/C–N lengths of **1′** are 1.314 Å, the experimental lengths are 1.319(3) Å at 296 K and 1.314(2) at 100 K. A plot of atomic spin densities obtained from Mulliken spin population analysis of **1′** are depicted in Figure 2 (a). It is observed that the beta spin (1.00) is only localized on the cobalt ion and that the alpha spin is delocalized over two ligands. This feature is consistent with Robin–Day Class III state, [$Co^{II}(L^{SPh}{}_{ISQ}{}^{0.5\bullet-})_2Cl$]. Thus, the results of this combined experimental and theoretical investigation indicate that [$Co^{II}(L^{SPh}{}_{ISQ}{}^{0.5\bullet-})_2X$] are the ground electronic states of the solids of **1–5**.

Complex [**1–5**]$^+$ ions are mixed-valence species of types [$Co^{III}(L^{SPh}{}_{IQ})(L^{SPh}{}_{ISQ}{}^{\bullet-})X$]$^+$. The delocalized states are [$Co^{III}(L^{SPh}{}_{ISQ}{}^{0.5\bullet-})_2X$]$^+$, as shown in Scheme S2. The EPR spectra confirmed that, in solutions, [**1–5**]$^+$ ions exhibit tautomeric equilibria of types [$Co^{III}(L^{SPh}{}_{ISQ}{}^{0.5\bullet-})_2X$]$^+$ ⇌ [$Co^{II}(L^{SPh}{}_{IQ})_2X$]$^+$. In CH_2Cl_2 at 296 K, they generate an isotropic EPR signal at $g \approx 2.000$ consistent with [$Co^{III}(L^{SPh}{}_{ISQ}{}^{0.5\bullet-})_2X$]$^+$ states. The isotropic (g = 2.001) EPR spectrum of **4**$^+$ ion at 296 K displays hyperfine couplings due to $^{57,59}Co$ (I = 7/2) nuclei, as illustrated in Figure S2. However, the EPR spectra of **1**$^+$ and **3**$^+$ in the frozen glass state, as depicted in Figure 3 (a and d), are anisotropic. The EPR signals at $g \approx 2.00$ due to $L^{SPh}{}_{ISQ}{}^{\bullet-}$ anion radical split in the frozen glass state and the corresponding g values are: **1**$^+$, g_1 = 1.972, g_2 = 2.193, g_3 = 2.409, Δg = 0.437; **3**$^+$, g_1 = 1.965, g_2 = 1.996, g_3 = 2.021 and Δg = 0.056. The g parameters and the anisotropy correlate with the higher contributions of [$Co^{II}(L^{SPh}{}_{IQ})_2X$]$^+$ states to the ground electronic states of [**1–5**]$^+$ ions at 115 K. The data supports the conclusion that **1–5** are hybrid states of [$Co^{III}(L^{SPh}{}_{ISQ}{}^{\bullet-})_2X$] and [$Co^{II}(L^{SPh}{}_{ISQ}{}^{0.5\bullet-})_2X$] tautomers.

DFT calculations on **1′**$^+$ ion predicted a similar trend. The calculated bond parameters of the doublet state are summarized in Table S5. A plot of atomic spin densities obtained from the Mulliken spin population analyses is illustrated in Figure 2

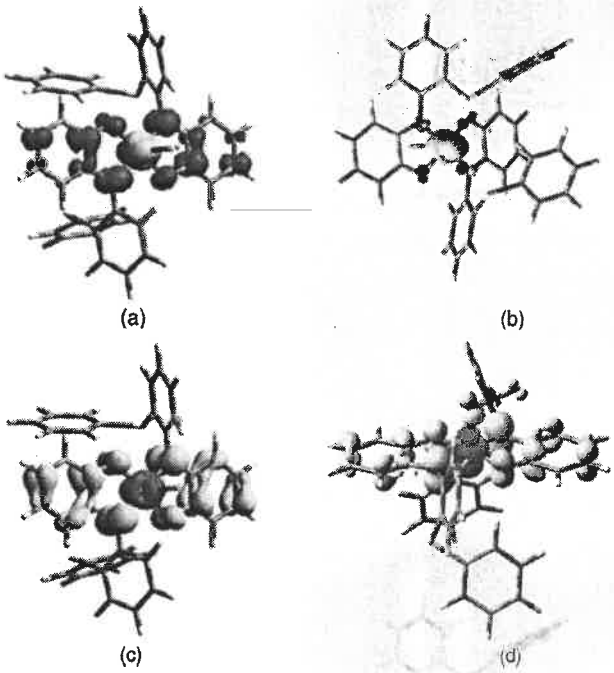

Figure 2. Spin density plots of (a) **1′**, (b) **1′**$^+$, (c) **1′**$^{\bullet-}$, and (d) **3′**$^{\bullet-}$ (yellow, α spin; red, β spin) and values from Mulliken spin population analyses (spin density, **1′**: Co1 1.006; Cl1 0.08; O1 –0.06; N8 –0.19; O31 –0.06; N38 –0.19; **1′**$^+$: Co1 0.87; Cl –0.01; O1 –0.01; O31 –0.01; **1′**$^{\bullet-}$: Co1 –0.78; O1 0.16; N8 0.36; O31 0.16; N38 0.36; **3′**$^{\bullet-}$: Co1 –0.67; O1 0.15; N8 0.32; O31 0.15; N38 0.34).

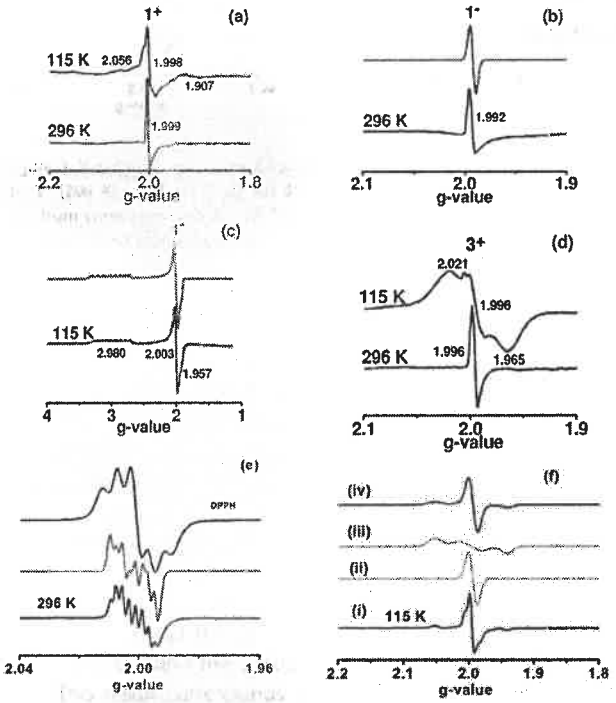

Figure 3. Variable-temperature X-band EPR spectra of (a) $\mathbf{1}^+$ (296 and 115 K), (b) $\mathbf{1}^-$ (296 K), (c) $\mathbf{1}^-$ (115 K), (d) $\mathbf{3}^+$ (296 and 115 K), (e) $\mathbf{3}^-$ (296 K, black spectrum corresponds to 2×10^{-4} M DPPH), and (f) $\mathbf{3}^-$ (115 K, the simulated spectrum (ii) is obtained considering $[Co^{III}(L^{SPh}{}_{ISQ}{}^{0.5\cdot-1.0-})_2N_3]^-$ state, the spectrum (iii) is generated considering $[Co^{II}(L^{SPh}{}_{ISQ}{}^{\cdot-})_2N_3]^-$ state and the spectrum (iv) is produced considering a hybrid state of these two (1:1) states) in CH_2Cl_2 (blue, experimental; red, simulated).

(b). Localization of the spin density predominantly on the cobalt ion (87 %) in the $\mathbf{1}^+$ ion inferred a major contribution of the $[Co^{II}(L^{SPh}{}_{IQ})_2X]^+$ states to the ground electronic states of $[\mathbf{1}\text{–}\mathbf{5}]^+$ ions, as determined from the frozen glass EPR spectra.

Complex $[\mathbf{1}\text{–}\mathbf{5}]^-$ ions are mixed-valence complexes of types $[Co^{III}(L^{SPh}{}_{AP}{}^{2-})(L^{SPh}{}_{ISQ}{}^{\cdot-})X]^-$ defined by $[Co^{III}(L^{SPh}{}_{ISQ}{}^{0.5\cdot-1.0-})_2X]^-$ states, as depicted in Scheme S2. Similar to $[\mathbf{1}\text{–}\mathbf{5}]^+$ ions, the EPR spectra of $[\mathbf{1}\text{–}\mathbf{5}]^-$ ions in CH_2Cl_2 are temperature dependent. The EPR spectra of the CH_2Cl_2 solutions of $[\mathbf{1}\text{–}\mathbf{5}]^-$ ions are isotropic at 296 K and the simulated g values in all cases are $g \approx 2.00$. This result corresponds to the electronic states of types $[Co^{III}(L^{SPh}{}_{ISQ}{}^{0.5\cdot-1.0-})_2X]^-$, which contain an uncoupled $L^{SPh}{}_{ISQ}{}^{\cdot-}$ anion radical. Similar to the $\mathbf{4}^+$ ion (Figure S2), the EPR spectrum of $\mathbf{3}^-$ ion exhibits hyperfine coupling due to ^{14}N ($I = 1$, $A = 2.5$ G) and $^{57,59}Co$ ($I = 7/2$, $A = 3.8$ G) nuclei and the signal was compared to that of DPPH (ca. 2×10^{-4} M in CH_2Cl_2) as illustrated in Figure 3 (e). The EPR spectra of the CH_2Cl_2 frozen glasses of $[\mathbf{1}\text{–}\mathbf{5}]^-$ are anisotropic. The frozen glass EPR spectra at 115 K of $\mathbf{1}^-$ and $\mathbf{3}^-$ ions are shown in Figure 3 (c and f). The anisotropic EPR spectrum of the CH_2Cl_2 frozen glass of $\mathbf{1}^-$ exhibits hyperfine splitting due to $^{57,59}Co$ ($I = 7/2$, $A_1 = 60$, $A_2 = 120$, $A_3 = 80$ G) nuclei. The data are consistent with the $[Co^{II}(L^{SPh}{}_{ISQ}{}^{\cdot-})_2Cl]^-$ state following the coupling scheme of type $[(L^{SPh}{}_{ISQ}{}^{\cdot-})\uparrow Co^{II}\uparrow(L^{SPh}{}_{ISQ}{}^{\cdot-})\downarrow]^-$ as observed in cases of bis(semiquinonate) complexes reported by Wieghardt and co-workers.[10f] The simulated g values of $\mathbf{1}^-$ ion are $g_1 = 1.957$, $g_2 = 2.003$, $g_3 = 2.980$ and $\Delta g = 1.02$. The cobalt-centered EPR spectrum of the frozen glass attributes the above coupling scheme only, the other coupling scheme $[(L^{SPh}{}_{ISQ}{}^{\cdot-})\uparrow Co^{II}\downarrow(L^{SPh}{}_{ISQ}{}^{\cdot-})\uparrow]^-$ correlates to the ligand-centered EPR spectra, which is observed in fluid solution. Notably, the frozen glass EPR spectrum of $\mathbf{3}^-$ ion was simulated satisfactorily by considering the contributions of the $[Co^{III}(L^{SPh}{}_{ISQ}{}^{0.5\cdot-1.0-})_2N_3]^-$ and $[Co^{II}(L^{SPh}{}_{ISQ}{}^{\cdot-})_2N_3]^-$ states. The isotropic EPR spectrum ($g = 1.998$), (ii) of Figure 3 (f) is due to $[Co^{III}(L^{SPh}{}_{ISQ}{}^{0.5\cdot-1.0-})_2N_3]^-$ component, whereas the anisotropic EPR spectrum ($g_1 = 1.941$, $g_2 = 1.998$, and $g_3 = 2.015$) (iii) was obtained by considering the contribution of the $[Co^{II}(L^{SPh}{}_{ISQ}{}^{\cdot-})_2N_3]^-$ component. The simulated spectrum (iv) was achieved by considering the hybrid (1:1) state of these two components. The feature is similar to that observed in the frozen glass and solid-state EPR spectra of **1**.

The calculated bond parameters of $\mathbf{1}^-$ and $\mathbf{3}^-$ ions are summarized in Tables S5 and S6. The plots of atomic spin densities of $\mathbf{1'}^-$ and $\mathbf{3'}^-$ are shown in Figure 2 (c and d). The calculated atomic spin densities indicate the co-existence of $[Co^{III}(L^{SPh}{}_{ISQ}{}^{0.5\cdot-1.0-})_2X]^-$ and $[Co^{II}(L^{SPh}{}_{ISQ}{}^{\cdot-})_2X]^-$ states in $[\mathbf{1}\text{–}\mathbf{5}]^-$ ions. The calculated atomic spin densities as shown in Figure 2 (c and d) disperse on both cobalt (–0.78 and –0.67 for $\mathbf{1'}^-$ and $\mathbf{3'}^-$) and the ligand backbone, indicating the co-existence of $[Co^{II}(L^{SPh}{}_{ISQ}{}^{\cdot-})_2X]^-$ and $[Co^{III}(L^{SPh}{}_{ISQ}{}^{0.5\cdot-1.0-})_2X]^-$ states in $[\mathbf{1}\text{–}\mathbf{5}]^-$ ions.

Electrochemical Study

The redox activities of **1**–**5** in CH_2Cl_2 were investigated by cyclic voltammetry at 296 K. The redox potential data referenced to the ferrocenium/ferrocene (Fc^+/Fc), couple are summarized in Table S7. The cyclic voltammograms are shown in Figure 4 and in the Supporting Information (Figure S3). The redox properties of **1**–**5** are similar, with all these complexes exhibiting two anodic redox waves and one cathodic wave. The analyses of the EPR spectra of the CH_2Cl_2 solutions of the electrogenerated species confirmed that $[\mathbf{1}\text{–}\mathbf{5}]^+$ and $[\mathbf{1}\text{–}\mathbf{5}]^-$ ions are cobalt(III) complexes of *o*-iminobenzosemiquinonate/*o*-iminobenzoquinone. The $[\mathbf{1}\text{–}\mathbf{5}]^+/[\mathbf{1}\text{–}\mathbf{5}]$ reduction waves at 0.16–0.34 V ($E_{1/2}{}^1$) depend marginally on the axial ligands, reflecting the minor contributions of $[Co^{II}(L^{SPh}{}_{ISQ}{}^{0.5\cdot-})_2X]$ states in solutions of **1**–**5**, which are defined by $[Co^{III}(L^{SPh}{}_{ISQ}{}^{\cdot-})_2X]$ electronic states. The isotropic EPR spectra correlate to the $[Co^{III}(L^{SPh}{}_{ISQ}{}^{0.5\cdot-})_2X]^+$ descriptions of $[\mathbf{1}\text{–}\mathbf{5}]^+$ ions. Thus, the first anodic waves of **1**–**5** are assigned to $L^{SPh}{}_{IQ}/L^{SPh}{}_{ISQ}{}^{\cdot-}$ oxidation couples. Similarly, the

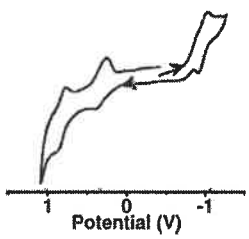

Figure 4. Cyclic voltammogram of **1** in CH_2Cl_2 at 296 K. Conditions: 0.2 M $[N(nBu)_4]PF_6$ supporting electrolyte; scan rate, 100 mV s^{-1}; platinum working electrode.

$[\mathbf{1–5}]^{2+}/[\mathbf{1–5}]^{+}$ redox waves at 0.73–0.83 V ($E_{1/2}^{2}$), are due to the $L^{SPh}{}_{IQ}/L^{SPh}{}_{ISQ}{}^{\bullet-}$ redox waves.

As the $[\mathbf{1–5}]^{-}$ ions are defined by $[Co^{III}(L^{SPh}{}_{ISQ}{}^{0.5\bullet-1.0-})_2X]^{-}$ descriptions, the cathodic waves of **1–5** at –0.76 to –1.03 V ($E_{1/2}^{3}$) are assigned to $L^{SPh}{}_{ISQ}{}^{\bullet-}/L^{SPh}{}_{AP}{}^{2-}$ reduction couples. The redox series of **1–5** are depicted in Scheme 6.

$$[Co^{III}(L^{SPh}{}_{IQ})_2X]^{2+} \underset{-e}{\overset{+e}{\rightleftharpoons}} [Co^{III}(L^{SPh}{}_{ISQ}{}^{0.5\bullet-})_2X]^{+}$$
$$[\mathbf{1–5}]^{2+} \qquad [\mathbf{1–5}]^{+}$$
$$\underset{-e}{\overset{+e}{\rightleftharpoons}} [Co^{III}(L^{SPh}{}_{ISQ}{}^{\bullet-})_2X] \underset{-e}{\overset{+e}{\rightleftharpoons}} [Co^{III}(L^{SPh}{}_{ISQ}{}^{0.5\bullet-1.0-})_2X]^{-}$$
$$[\mathbf{1–5}] \qquad [\mathbf{1–5}]^{-}$$

Scheme 6. Redox series of **1–5**.

Electronic Spectra, Spectroelectrochemical Measurements and Time-Dependent (TD) DFT Calculations

UV/Vis/NIR absorption spectra of $L^{SPh}H_2$ and **1–5** were recorded in CH_2Cl_2 at 296 K. The spectrum of $L^{SPh}H_2$ is shown in Figure S4 and the spectra of the complexes are shown in Figure 5. The absorption spectroscopic data are summarized in Table S8. The UV/Vis absorption spectra in CH_2Cl_2 depend on temperature, as illustrated in Figure S5. The general trend is that with a decrease of temperature, the intensity of the bands > 600 nm increases. TD DFT calculations were employed to explore the excitation parameters of **1′** in CH_2Cl_2 by using the CPCM model. The ability of TD DFT calculations to predict charge-transfer transitions has limitations;[14] however, it is used to predict approximately the transition types. The excitation energies with the oscillator strengths and the transition types are summarized in Table S9.

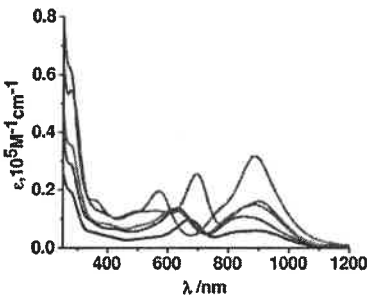

Figure 5. Electronic spectra of **1** (black), **2** (red), **3** (blue), **4** (green), and **5** (pink) in CH_2Cl_2 at 296 K.

In solution, the absorption at 685 nm due to MMLLCT is stronger than that at 1022 nm because of MLCT. The electronic spectra of **1–5** are similar, exhibiting two lower energy absorption bands in the ranges of 850–900 and 615–765 nm (Table S8). The calculated wavelength of **1** at 928 nm is due to the $d_{Co} + \pi_{ISQ} \rightarrow \pi_{ISQ}$ transitions. In solutions, the excitations are dominantly due to $L^{SPh}{}_{ISQ}{}^{\bullet-} \rightarrow L^{SPh}{}_{ISQ}{}^{\bullet-}$ (charge resonance transfer) transitions, which are invariant on the types of axial ligands. Similar types of transitions for planar bis(semiquinone) complexes were predicted by Wieghardt, Neese, and co-workers.[1f]

The electronic spectra of $[\mathbf{1–5}]^{+}$, $[\mathbf{1–5}]^{2+}$, and $[\mathbf{1–5}]^{-}$ were obtained from spectroelectrochemical measurements in CH_2Cl_2 at 296 K. The change of electronic spectra with several isosbestic points during the redox reactions are shown in Figure 6 and Figure S6. The general trend is that during oxidation or reduction, the intensities of the λ_{max} of the original complexes gradually decrease.

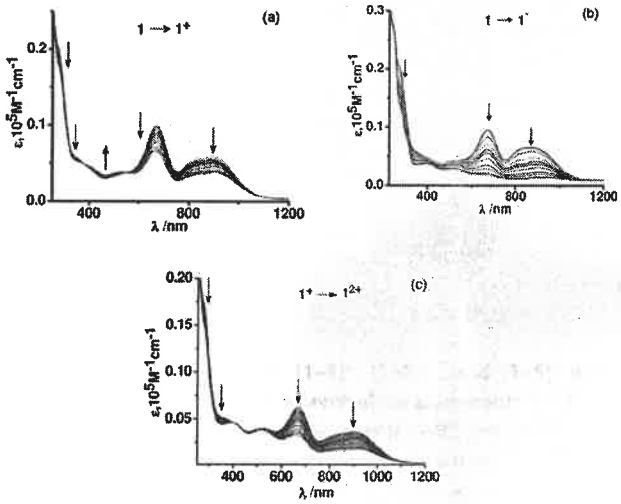

Figure 6. Spectroelectrochemical measurements showing the change of electronic spectra during the conversions of $\mathbf{1} \rightarrow [\mathbf{1}]^{n}$ (n = 1⁺, 1⁻) in CH_2Cl_2 at 296 K.

The results are consistent with the di-radical singlet states of complexes **1–5** , which absorb strongly in the NIR region due to spin-allowed ($\Delta S = 0$) and dipole-allowed ($\Delta\mu \neq 0$) $[(L^{SPh}{}_{ISQ}{}^{\bullet-})\text{-}M(L^{SPh}{}_{ISQ}{}^{\bullet-})] \rightarrow [(L^{SPh}{}_{IQ})M(L^{SPh}{}_{AP}{}^{2-})]$ transitions. Another feature is that the absorption maxima of the cations and anions are relatively broad and that the λ_{max} are redshifted in comparison to those of the neutral analogues. In fluid solutions, $[\mathbf{1–5}]^{+}$ ions absorb due to $L^{SPh}{}_{ISQ}{}^{\bullet-} \rightarrow L^{SPh}{}_{IQ}$ transitions, whereas in $[\mathbf{1–5}]^{-}$ ions the charge transfers are due to $L^{SPh}{}_{AP}{}^{2-} \rightarrow L^{SPh}{}_{ISQ}{}^{\bullet-}$ and $L^{SPh}{}_{AP}{}^{2-} \rightarrow M^{2+/3+}$ transitions. The $\Delta\mu$ are closer to zero for $[(L^{SPh}{}_{ISQ}{}^{\bullet-})M(L^{SPh}{}_{IQ})]^{+} \rightarrow [(L^{SPh}{}_{IQ})M(L^{SPh}{}_{ISQ}{}^{\bullet-})]^{+}$ and $[(L^{SPh}{}_{ISQ}{}^{\bullet-})\text{-}M(L^{SPh}{}_{AP}{}^{2-})]^{-} \rightarrow [(L^{SPh}{}_{AP}{}^{2-})M(L^{SPh}{}_{ISQ}{}^{\bullet-})]^{-}$ transitions, which occur at lower energies, and the intensities of the absorptions decrease upon oxidation or reduction.

Solid-State Electronic Spectra

The solid-state absorption spectra (Kubelka–Munk plot)[15] of **1–5** were recorded by using the diffuse reflection method at 296 K; the spectra are shown in Figure 7. The significant absorption peaks of solids are summarized in Table S8. The electronic spectra of solids are different from those of CH_2Cl_2 solutions (Figure 5). The spectra of solids are broad and are composed of multiple Gaussian components. They display NIR absorption bands that are absent in solutions. The solid-state electronic spectra of **1–5** exhibit absorption bands at > 1000 nm that are absent in solutions. The NIR absorption bands of **1–5** depend significantly on the axial ligands and appear at 1502, 1360, 1485, 1202, and 1354 nm, which are assigned to co-

balt(II) → L^{SPh}_{IQ} transitions. In CH_2Cl_2, the $L^{SPh}_{ISQ}{}^{\bullet-} \rightarrow L^{SPh}_{ISQ}{}^{\bullet-}$ (charge resonance transfer) transitions appear at 890, 880, 851, 881, and 900 nm, whereas in solids they are bathochromically shifted to 1047, 1022, 1041, 1078, and 980 nm. The MLCT and (charge resonance transfer) transition features are consistent with the existence of Robin–Day Class III complexes of type *trans*-$[Co^{II}(L^{SPh}_{ISQ}{}^{0.5\bullet-})_2X]$ in the solids of **1–5**.

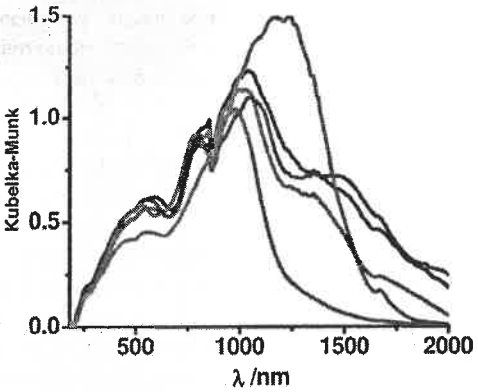

Figure 7. Solid-state UV/Vis/NIR spectra of **1** (black), **2** (red), **3** (blue), **4** (green), and **5** (pink) at 296 K.

Conclusions

The precise assignment of the electronic state of an iminobenzosemiquinonate anion radical ($L^{NO}_{ISQ}{}^{\bullet-}$) coordinated to a redox-active transition-metal ion is complex; indeed, it becomes more complex in the case of bis($L^{NO}_{ISQ}{}^{\bullet-}$) complexes. In this article, mixed-valence complexes of 2,4-di-*tert*-butyl-*N*-[2-(phenylthio)]phenyl-*o*-iminobenzosemiquinonate anion radical ($L^{SPh}_{ISQ}{}^{\bullet-}$) and its quinone state (L^{SPh}_{IQ}) with cobalt ions were disclosed. Neutral bis(ligand) complexes constitute a family of mixed-valence complexes of type $[Co^{II}(L^{SPh}_{ISQ}{}^{\bullet-})(L^{SPh}_{IQ})X]$ defined by delocalized Robin–Day Class III states, *trans*-$[Co^{II}(L^{SPh}_{ISQ}{}^{0.5\bullet-})_2X]$ {X = Cl^-, **1**; SCN^- (thiocyanato-*kS*), **2**; N_3^-, **3**; NO_2^-, **4** and I_3^-, **5**}. The average C–O/N lengths (1.335 ± 0.010 Å for $L^{SPh}_{ISQ}{}^{\bullet-}$ and 1.308 ± 0.01 Å for $L^{SPh}_{ISQ}{}^{0.5\bullet-}$ states), which are a measure of the contribution of $L^{SPh}_{ISQ}{}^{\bullet-}/L^{SPh}_{IQ}$ states in crystals, are: **1**, 1.319(3); **2**, 1.320(2); **3**, 1.322(3); **4**, 1.322(2); **5**, 1.315(6) Å. The shorter average C–O/N lengths than those of $L^{NO}_{ISQ}{}^{\bullet-}$ and the localization of the beta spin exclusively on cobalt ion and alpha spin equally on two ON-chelates obtained from the BS solution confirmed the mixed-valence states of **1–5**. The temperature-dependent X-ray bond parameters and the MLCT absorption bands in solids, which are absent in solutions, inferred that **1–5** exhibit tautomeric equilibria of $[Co^{III}(L^{SPh}_{ISQ}{}^{\bullet-})_2] \rightleftharpoons [Co^{II}(L^{SPh}_{ISQ}{}^{0.5\bullet-})_2]$ states. Similarly, $[\mathbf{1–5}]^+$ and $[\mathbf{1–5}]^-$ are mixed-valence complex ions that exhibit tautomeric equilibria of type $[Co^{III}(L^{SPh}_{ISQ}{}^{\bullet-})_2]^+ \rightleftharpoons [Co^{II}(L^{SPh}_{IQ})_2]^+$ and $[Co^{III}(L^{SPh}_{ISQ}{}^{0.5\bullet-1.0-})_2]^- \rightleftharpoons [Co^{II}(L^{SPh}_{ISQ}{}^{\bullet-})_2]^-$. The isotropic EPR signals of CH_2Cl_2 solutions of $[\mathbf{1–5}]^+$ at 296 K at $g \approx 2.00$ correlate with the existence of $[Co^{III}(L^{SPh}_{ISQ}{}^{0.5\bullet-})_2X]^+$ states in solutions, whereas the anisotropy EPR signals of the frozen glasses at 115 K at $g \approx 1.97–2.41$ are due to $[Co^{II}(L^{SPh}_{IQ})_2X]^+$ states. The variable-temperature EPR spectra established that, in solutions, $[\mathbf{1–5}]^-$ exist exclusively as $[Co^{III}(L^{SPh}_{ISQ}{}^{0.5\bullet-1.0-})_2X]^-$, whereas in frozen glasses the $[Co^{II}(L^{SPh}_{ISQ}{}^{\bullet-})_2X]^-$ states dominate.

Experimental Section

Materials and Physical Measurements

General: Reagents or analytical grade materials were obtained from commercial suppliers and used without further purification. Spectroscopic grade solvents were used for spectroscopic and electrochemical measurements. The C, H and N content of the compounds were obtained with a Perkin–Elmer 2400 Series II elemental analyzer. Infrared spectra of the samples were measured from 4000 to 400 cm^{-1} with KBr pellets at room temperature with a Perkin–Elmer Spectrum RX 1 FTIR spectrophotometer. ^1H NMR spectra in $CDCl_3$ solvent were obtained at 296 K with a Bruker DPX 300 MHz spectrometer. ESI mass spectra were recorded with a micro mass Q-TOF mass spectrometer. Electronic absorption spectra in solution were obtained with a Perkin–Elmer Lambda 750 spectrophotometer in the range 3300–175 nm. The X-band EPR spectra were measured with a Magnettech GmbH MiniScope MS400 spectrometer (equipped with temperature controller TC H03), where the microwave frequency was measured with an FC400 frequency counter. The EPR spectra were simulated by using EasySpin software. For electroanalytical investigations, a BASi Epsilon-EC instrument was used for cyclic voltammetric experiments in CH_2Cl_2 solutions containing 0.2 M tetrabutylammonium hexafluorophosphate as supporting electrolyte. The BASi platinum working electrode, platinum auxiliary electrode, and Ag/AgCl reference electrode were used for the measurements. The redox potential data are referenced vs. ferrocenium/ferrocene (Fc^+/Fc) couple. BASi SEC-C thin-layer quartz glass spectroelectrochemical cell kits (light path length of 1 mm) with platinum gauze working electrode and SEC-C platinum counter electrode were used for spectroelectrochemistry measurements.

2,4-Di-*tert*-butyl-6-{[2-(phenylthio)phenyl]amino}phenol ($L^{SPh}H_2$): To a solution of 3,5-di-*tert*-butylcatechol (1.1 g, 5 mmol) and triethylamine (0.3 mL) in *n*-hexane (150 mL), 2-(phenylthio)aniline (1.0 g; 5 mmol) was added. The resulting mixture was stirred in air for 3 d. A reddish oily solution was obtained, which was poured on a basic alumina column. Elution with a mixture of chloroform and *n*-hexane solvents (1:5) afforded pure $L^{SPh}H_2$ ligand, yield 1.72 g (ca. 84 % with respect to catechol). ^1H NMR (300 MHz, $CDCl_3$): δ = 7.18–7.30 (m, 4 H), 6.94–6.98 (m, 3 H), 6.59–6.61 (d, 2 H), 6.30 (br., 2 H), 5.08 (s, 2 H), 1.39 (s, 9 H), 1.22 (s, 9 H) ppm. ^{13}C NMR (75 MHz, $CDCl_3$): δ = 149.6, 146.8, 145.8, 142.2, 137.2, 136.6, 131.1, 130.8, 129.3, 129.0, 128.8, 126.8, 125.9, 124.0, 122.5, 120.5, 116.2, 115.3, 114.1, 109.8, 34.9, 34.7, 29.8, 29.43 ppm. IR (KBr): $\tilde{\nu}$ = 3435 (m, NH), 3058 (s, *t*Bu), 2957 (s, *t*Bu), 1587 (s), 1477 (s), 1421 (s), 1310 (m), 1221 (m), 1024 (s), 738 (s), 690 (s) cm^{-1}.$C_{26}H_{31}NOS$ (405.21): calcd. C 76.99, H 7.70, N 3.45; found C 76.75, H 7.66, N 3.43. MS (EI-MS): *m/z* = 405 $[L^{SPh}H_2]^+$.

***trans*-$[Co^{II}(L^{SPh}_{ISQ}{}^{0.5\bullet-})_2Cl]$ (1):** To a solution of $L^{SPh}H_2$ (200 mg, 0.5 mmol) in anhydrous CH_3OH (15 mL) in a 100 mL round-bottom flask, anhydrous $CoCl_2$ (34 mg, 0.25 mmol) was added and the solution was stirred for 10 min in air. The solution was allowed to evaporate slowly in air. After 2–3 d, the mixture became violet and black crystals of **1** separated out, which were collected upon filtration and dried in air (crystals for single-crystal X-ray diffraction measurement were collected from this crop), yield 120 mg (53 % with respect to Co). ^1H NMR (300 MHz, $CDCl_3$): δ = 8.34 (t, 2 H), 7.49 (t, 4 H), 7.28–7.41 (m, 6 H), 7.24 (d, 2 H), 7.16 (d, 2 H), 7.01 (d, 4 H), 6.94 (s, 2 H), 1.39 (s, 18 H), 1.22 (s, 18 H) ppm. ^{13}C NMR (75 MHz, $CDCl_3$):

δ = 184.9, 167.4, 151.2, 148.6, 145.6, 134.6, 132.9, 131.8, 128.8, 127.9, 127.0, 126.85, 126.1, 125.06, 124.5, 114.5, 35.6, 34.7, 29.5, 29.43 ppm. IR (KBr): $\tilde{\nu}$ = 3054 (s, Ar–H), 2957 (vs, *t*Bu), 2902 (s, *t*Bu), 2867 (m, *t*Bu), 1573 (m), 1509 (m), 1487 (vs), 1330 (m), 1022 (vs), 746 (vs) cm^{-1}. MS (ESI, positive ion, CH_3OH): *m/z* = 865.81 [**1**-Cl]$^+$. $C_{52}H_{58}ClCoN_2O_2S_2$ (901.55): calcd. C 69.28, H 6.48, N 3.11; found C 69.22, H 6.46, N 3.09.

***trans*-[Co^{III}(L$^{SPh}_{ISQ}$$^{0.5-}$)$_2$SCN] (2):** To a solution of L^{SPh}H$_2$ (200 mg, 0.5 mmol) in anhydrous CH_3OH (15 mL) in a 100 mL round-bottom flask, anhydrous $CoCl_2$ (34 mg, 0.25 mmol) and NaSCN (81 mg, 1 mmol) were successively added and the solution was stirred for 10 min in air. The solution was allowed to evaporate slowly in air. After 2–3 d the mixture became violet and black crystals of **2** separated out, which were collected upon filtration and dried in air (crystals for single-crystal X-ray diffraction measurement were collected from this crop), yield 145 mg (64 % with respect to Co). ^{1}H NMR (300 MHz, $CDCl_3$): δ = 7.95 (t, 2 H), 7.52 (t, 4 H), 7.29–7.45 (m, 6 H), 7.25 (d, 2 H), 7.17 (d, 2 H), 7.04–7.12 (m, 4 H), 6.94 (s, 2 H), 1.39 (s, 18 H), 1.22 (s, 18 H) ppm. ^{13}C NMR (75 MHz, $CDCl_3$): δ = 182.8, 168.2, 152.4, 147.7, 146.4, 134.5, 132.5, 132.0, 128.6, 128.1, 127.6, 127.4, 127.2, 126.9, 126.5, 123.4, 114.5, 35.7, 34.7, 28.9, 28.2 ppm. IR (KBr): $\tilde{\nu}$ = 3058 (m, Ar–H), 2959 (s, *t*Bu), 2908 (s, *t*Bu), 2866 (m, *t*Bu), 2101 (vs, –SCN), 1639 (s), 1580 (s), 1529 (s), 1471 (s), 1361 (vs), 1306 (s), 1104 (vs), 1022 (s), 751 (vs) cm^{-1}. MS (ESI, positive ion, CH_3OH): *m/z* = 865.81 [**2**-SCN]$^+$. $C_{53}H_{58}CoN_3O_2S_3$ (924.17): calcd. C 68.88, H 6.33, N 4.55; found C 68.81, H 6.31, N 4.52.

***trans*-[Co^{III}(L$^{SPh}_{ISQ}$$^{0.5-}$)$_2N_3$] (3):** To a solution of L^{SPh}H$_2$ (200 mg, 0.5 mmol) in anhydrous CH_3OH (15 mL) in a 100 mL round-bottom flask, anhydrous $CoCl_2$ (34 mg, 0.25 mmol) and NaN_3 (56 mg, 1 mmol) were successively added and the solution was stirred for 10 min in air. The solution was allowed to evaporate slowly in air. After 2–3 d the mixture became violet and black crystals of **3** separated out, which were collected upon filtration and dried in air (crystals for single-crystal X-ray diffraction measurement were collected from this crop), yield 125 mg (55 % with respect to Co). ^{1}H NMR (300 MHz, $CDCl_3$): δ = 7.99 (m, 2 H), 7.76 (d, 2 H), 7.28–7.43 (m, 8 H), 7.26 (d, 2 H), 7.19 (d, 2 H), 7.08–7.15 (m, 4 H), 6.98 (s, 2 H), 1.39 (s, 18 H), 1.22 (s, 18 H) ppm. ^{13}C NMR (75 MHz, $CDCl_3$): δ = 185.2, 167.1, 151.2, 148.3, 145.5, 134.2, 132.5, 131.5, 130.9, 128.8, 128.1, 127.8, 127.1, 126.3, 125.2, 114.0, 35.1, 34.5, 29.5, 29.2 ppm. IR (KBr): $\tilde{\nu}$ = 3063 (m, Ar–H), 2954 (vs, *t*Bu), 2903 (s, *t*Bu), 2864 (m, *t*Bu), 1983 (vs, –N$_3$), 1580 (s), 1526 (m), 1471 (vs), 1364 (vs), 1303 (s), 1029 (m), 734 (vs) cm^{-1}. MS (ESI, positive ion, CH_3OH): *m/z* = 865.81 [**3**-N$_3$]$^+$. $C_{52}H_{58}CoN_5O_2S_2$ (908.12): calcd. C 68.78, H 6.44, N 7.71; found C 68.72, H 6.40, N 7.69.

***trans*-[Co^{III}(L$^{SPh}_{ISQ}$$^{0.5-}$)$_2$(NO$_2$)] (4):** To a solution of L^{SPh}H$_2$ (200 mg, 0.5 mmol) in anhydrous CH_3OH (15 mL) in a 100 mL round-bottom flask, anhydrous $CoCl_2$ (34 mg, 0.25 mmol) and $NaNO_2$ (69 mg, 1 mmol) were successively added and the solution was stirred for 10 min in air. The solution was allowed to evaporate slowly in air. After 2–3 d the mixture became violet and black crystals of **4** separated out, which were collected upon filtration and dried in air (crystals for single-crystal X-ray diffraction measurement were collected from this crop), yield 155 mg (67 % with respect to Co). ^{13}C NMR (75 MHz, $CDCl_3$): δ = 185.0, 167.4, 151.3, 148.7, 145.7, 134.6, 132.9, 131.9, 130.8, 128.8, 127.6, 127.4, 126.8, 126.1, 125.1, 114.5, 35.6, 34.7, 29.5, 29.43 ppm. IR (KBr): $\tilde{\nu}$ = 3073 (m, Ar–H), 2954 (vs, *t*Bu), 2895 (s, *t*Bu), 2865 (s, *t*Bu), 1639 (m), 1570 (m), 1525 (s), 1471 (vs), 1412 (vs), 1361 (vs), 1284 (vs, –NO$_2$), 1250 (m, –NO$_2$), 1094 (m), 1022 (m), 748 (vs) cm^{-1}. MS (ESI, positive ion, CH_3OH): *m/z* = 865.81 [**4**-NO$_2$]$^+$. $C_{52}H_{58}CoN_3O_4S_2$ (912.10): calcd. C 68.47, H 6.41, N 4.61; found C 68.42, H 6.39, N 4.59. ^{1}H NMR (300 MHz, $CDCl_3$): δ = 8.34 (t, 2 H), 7.49 (t, 4 H), 7.28–7.41 (m, 6 H), 7.24 (d, 2 H), 7.14 (d, 2 H), 7.03 (d, 4 H), 6.98 (s, 2 H), 1.33 (s, 18 H), 1.24 (s, 18 H) ppm.

***trans*-[Co^{III}(L$^{SPh}_{ISQ}$$^{0.5-}$)$_2I_3$] (5):** To a solution of **3** (100 mg, 0.1 mmol) in CH_2Cl_2 (20 mL) was added a solution of I_2 (25 mg, 0.1 mmol) in *n*-hexane (20 mL), and the solution was allowed to diffuse at 296 K. After 4–5 d, black needles of **5** separated out, which were filtered and dried in air (single crystals for X-ray diffraction were collected from these products), yield 56 mg (53 % with respect to **3**). ^{1}H NMR (300 MHz, $CDCl_3$): δ = 7.99 (t, 2 H), 7.49 (t, 4 H), 7.28–7.41 (m, 6 H), 7.24 (d, 2 H), 7.14 (d, 2 H), 7.03 (d, 4 H), 6.98 (s, 2 H), 1.33 (s, 18 H), 1.24 (s, 18 H) ppm. IR (KBr): $\tilde{\nu}$ = 3054 (s, Ar–H), 2954 (vs, *t*Bu), 2900 (s, *t*Bu), 2860 (m, *t*Bu), 1573 (m), 1509 (m), 1487 (vs), 1330 (m), 1022 (vs), 746 (vs) cm^{-1}. MS (ESI, positive ion, CH_2Cl_2): *m/z* = 685.8 [**5**]$^+$. $C_{52}H_{58}CoI_3O_4S_2$ (1250.79): calcd. C 50.09, H 4.69, N 2.25; found C 50.02, H 4.67, N 2.24.

Complexes [1–5]$^+$ and [1–5]$^-$: These complexes were not isolated in this investigation. However, they were generated by coulometric experiments in CH_2Cl_2 at 296 K for spectroelectrochemical measurements and EPR spectra. Complexes **1**$^+$, **2**$^+$, **3**$^+$, and **4**$^+$ were generated upon oxidation of **1**, **2**, **3**, and **4**, respectively, at +0.56, +0.56, +0.54, and +0.59 V with respect to Fc^+/Fc couple, whereas **1**$^-$, **2**$^-$, **3**$^-$, and **4**$^-$ were produced upon reduction of **1**, **2**, **3**, and **4**, respectively, at –1.06, –1.05, –1.19, and –1.10 V, respectively.

Single-Crystal X-ray Structure Determination

Single crystals of **1–5** were picked up with nylon loops and mounted on Bruker APEX-II CCD and Bruker AXS D8 QUEST ECO diffractometers equipped with a Mo-target rotating-anode X-ray source and a graphite monochromator (Mo-K_α, λ = 0.71073 Å). Final cell constants were obtained from least-squares fits of all measured reflections. Intensity data were corrected for absorption by using the intensities of redundant reflections. The structures were readily solved by direct methods and subsequent difference Fourier techniques. The crystallographic data are listed in Table S1. The Siemens SHELXS-97[16] software package was used for solution, and SHELXL-97[16] was used for the refinement and XS. Ver. 2013/1,[17a] XT. Ver. 2014/4,[17b] and XL. Ver. 2014/7[17c] was used for the structure solution and refinement. All non-hydrogen atoms were refined anisotropically. Hydrogen atoms were placed at the calculated positions and refined as riding atoms with isotropic displacement parameters.

CCDC 1451720 (for **1**, 100 K), 1451721 (for **1**, 296 K), 1451722 (for **2**), 1451723 (for **3**), 1451724 (for **4**), and 1451725 (for **5**) contain the supplementary crystallographic data for this paper. These data can be obtained free of charge from The Cambridge Crystallographic Data Centre.

Density Functional Theory (DFT) Calculations

All calculations reported in this article were performed with the Gaussian 03W[18] program package supported by GaussView 4.1. The DFT[19] and TD DFT[20] calculations were performed at the level of Becke three parameter hybrid functional with the non-local correlation functional of Lee–Yang–Parr (B3LYP).[21] Gas-phase geometries of [Co(L$^{SPh-tBu}$)$_2$Cl] (**1′**), [Co(L$^{SPh-tBu}$)$_2$N$_3$] (**3′**), with singlet spin state, and [Rh(L$^{SPh-tBu}$)(PMe$_3$)Cl$_2$] (**1^{Me}′**), [Co(L$^{SPh-tBu}$)$_2$Cl]$^+$ (**1′**$^+$), [Co(L$^{SPh-tBu}$)$_2$Cl]$^-$ (**1′**$^-$), and [Co(L$^{SPh-tBu}$)$_2$N$_3$]$^-$ (**3′**$^-$), with doublet spin state, were optimized by using Pulay's Direct Inversion[22] in the Iterative Subspace (DIIS), "tight" convergent SCF procedure,[23] ignoring symmetry. As the closed shell singlet state solutions of **1′** was unstable, broken symmetry (BS) DFT calculations were performed so that **1′** would have stable solutions. To compare with the doublet spin state, the gas-phase geometry of **3′**$^-$ was also optimized with quartet spin state. In all calculations, the LANL2DZ basis set along with the corresponding effective core potential (ECP) was

used for ruthenium, cobalt, and rhodium.[24] Valence double zeta basis set, 6-31G[25] for H was used. For C, N, Cl, and P non-hydrogen atoms, valence double zeta with diffuse and polarization functions, 6-31+G* as basis set[26] was employed for all calculations. The percentage contributions of metal and ligands to the frontier orbitals were calculated by using the GaussSum program package.[27] The sixty lowest singlet excitation energies on each of the optimized geometries of **1'** in CH_2Cl_2 using CPCM model[28] were calculated by using the TD DFT method.

Acknowledgments

Financial support was received from the Department of Science and Technology (DST), New Delhi (SR/S1/IC/0026/2012) and the Council of Scientific and Industrial Research (CSIR), New Delhi (2699/12/EMR-II). S. M., S. B. and S. K. are thankful to CSIR for fellowships.

Keywords: Redox chemistry · Radical ions · Mixed-valent compounds · Tautomerism · Cobalt

[1] a) G. Skara, B. Pinter, P. Geerlings, F. De Proft, *Chem. Sci.* **2015**, *6*, 4109–4117; b) A. B. P. Lever, *Coord. Chem. Rev.* **2010**, *254*, 1397–1405; c) D. Kiriya, K. Nakamura, H.-C. Chang, S. Kitagawa, *Chem. Commun.* **2009**, 4085–4087; d) C. Remenyi, M. Kaupp, *J. Am. Chem. Soc.* **2005**, *127*, 11399–11413; e) S. Noro, H.-C. Chang, T. Takenobu, T. Akutagawa, D. Tanaka, T. Nakamura, S. Kitagawa, Y. Iwasa, T. Aoyama, T. Sassa, T. Wada, *J. Am. Chem. Soc.* **2005**, *127*, 10012–10013; f) D. Herebian, K. Wieghardt, F. Neese, *J. Am. Chem. Soc.* **2003**, *125*, 10997–11005; g) P. Chaudhuri, C. N. Verani, E. Bill, E. Bothe, T. Weyhermüller, K. Wieghardt, *J. Am. Chem. Soc.* **2001**, *123*, 2213–2223.

[2] a) D. L. J. Broere, R. Plessius, J. I. van der Vlugt, *Chem. Soc. Rev.* **2015**, *44*, 6886–6915; b) O. R. Luca, R. H. Crabtree, *Chem. Soc. Rev.* **2013**, *42*, 1440–1459; c) V. Lyaskovskyy, B. de Bruin, *ACS Catal.* **2012**, *2*, 270–279.

[3] a) J. L. Wong, R. F. Higgins, I. Bhowmick, D. X. Cao, G. Szigethy, J. W. Ziller, M. P. Shores, A. F. Heyduk, *Chem. Sci.* **2016**, *7*, 1594–1599; b) A. Witt, F. W. Heinemann, M. M. Khusniyarov, *Chem. Sci.* **2015**, *6*, 4599–4609; c) J. Takaichi, Y. Morimoto, K. Ohkubo, C. Shimokawa, T. Hojo, S. Mori, H. Asahara, H. Sugimoto, N. Fujieda, N. Nishiwaki, S. Fukuzumi, S. Itoh, *Inorg. Chem.* **2014**, *53*, 6159–6169, and references cited therein; d) H.-C. Chang, S. Kitagawa, *Angew. Chem. Int. Ed.* **2002**, *41*, 130–133; *Angew. Chem.* **2002**, *114*, 138.

[4] a) C. G. Pierpont, *Coord. Chem. Rev.* **2001**, *216–217*, 99; b) C. G. Pierpont, R. M. Buchanan, *Coord. Chem. Rev.* **1981**, *38*, 45.

[5] a) M. M. Khusniyarov, T. Weyhermüller, E. Bill, K. Wieghardt, *J. Am. Chem. Soc.* **2009**, *131*, 1208–1221; b) S. Kokatam, T. Weyhermüller, E. Bothe, P. Chaudhuri, K. Wieghardt, *Inorg. Chem.* **2005**, *44*, 3709–3717; c) K. S. Min, T. Weyhermüller, E. Bothe, K. Wieghardt, *Inorg. Chem.* **2004**, *43*, 2922–2931.

[6] a) F. Novio, E. Evangelio, N. Vazquez-Mera, P. González-Monje, E. Bellido, S. Mendes, N. Kehagias, D. Ruiz-Molina, *Sci. Rep.* **2013**, *3*, 1708; b) N. Azzaroli, A. Lapini, M. D. Donato, A. Dei, R. Righini, *J. Phys. Chem. B* **2013**, *117*, 15492–15502; c) O. S. Jung, C. G. Pierpont, *J. Am. Chem. Soc.* **1994**, *116*, 2229–2230.

[7] a) H.-C. Chang, D. Kiriya, *Eur. J. Inorg. Chem.* **2013**, 642–652; b) C. G. Pierpont, *Inorg. Chem.* **2011**, *50*, 9766–9772; c) D. Kiriya, H.-C. Chang, K. Nakamura, D. Tanaka, K. Yoneda, S. Kitagawa, *Chem. Mater.* **2009**, *21*, 1980–1988; d) D. Kiriya, K. Nakamura, H.-C. Chang, S. Kitagawa, *Chem. Commun.* **2009**, 4085–4087.

[8] a) N. Kundu, M. Maity, P. B. Chatterjee, S. J. Teat, A. Endo, M. Chaudhury, *J. Am. Chem. Soc.* **2011**, *133*, 20104–20107; b) E. Evangelio, D. Ruiz-Molina, *C. R. Acad. Sci., Ser. IIc* **2008**, *11*, 1137–1154.

[9] A. Rajput, A. K. Sharma, S. K. Barman, D. Koley, M. Steinert, R. Mukherjee, *Inorg. Chem.* **2014**, *53*, 36–48.

[10] a) A. I. Poddel'sky, M. P. Bubnov, G. K. Fukin, V. K. Cherkasov, G. A. Z. Abakumov, *Z. Anorg. Allg. Chem.* **2008**, *634*, 1205–1209; b) S.-L. Kokatam, P. Chaudhuri, T. Weyhermüller, K. Wieghardt, *Dalton Trans.* **2007**, 373–378; c) G. A. Abakumov, V. K. Cherkasov, M. P. Bubnov, L. G. Abakumova, V. N. Ikorskii, G. V. Romanenko, A. I. Poddel'sky, *Russ. Chem. Bull. Int. Ed.* **2006**, *55*, 44–52; d) E. Bill, E. Bothe, P. Chaudhuri, K. Chlopek, D. Herebian, S. Kokatam, K. Ray, T. Weyhermüller, F. Neese, K. Wieghardt, *Chem. Eur. J.* **2005**, *11*, 204–224; e) A. I. Poddel'sky, V. K. Cherkasov, G. K. Fukin, M. P. Bubnov, L. G. Abakumova, G. A. Abakumov, *Inorg. Chim. Acta* **2004**, *357*, 3632–3640; f) H. Chun, E. Bill, E. Bothe, T. Weyhermüller, K. Wieghardt, *Inorg. Chem.* **2002**, *41*, 5091–5099; g) X. Sun, H. Chun, K. Hildenbrand, E. Bothe, T. Weyhermüller, F. Neese, K. Wieghardt, *Inorg. Chem.* **2002**, *41*, 4295–4303; h) D. Herebian, P. Ghosh, H. Chun, E. Bothe, T. Weyhermüller, K. Wieghardt, *Eur. J. Inorg. Chem.* **2002**, 1957–1967; i) H. Chun, E. Bill, T. Weyhermüller, K. Wieghardt, *Angew. Chem. Int. Ed.* **2001**, *40*, 2489–2492; *Angew. Chem.* **2001**, *113*, 2552.

[11] A. I. Poddel'sky, V. K. Cherkasov, G. A. Abakumov, *Coord. Chem. Rev.* **2009**, *253*, 291–324.

[12] S. Kundu, S. Maity, T. Weyhermüller, P. Ghosh, *Inorg. Chem.* **2013**, *52*, 7417–7430.

[13] a) S. Jie, S. Zhang, K. Wedeking, W. Zhang, H. Ma, X. Lu, Y. Deng, W.-H. Sun, *C. R. Acad. Sci., Ser. IIc* **2006**, *9*, 1500–1509; b) S. Wang, B. Li, T. Liang, C. Redshaw, Y. Li, W.-H. Sun, *Dalton Trans.* **2013**, *42*, 9188–9197.

[14] a) Y. Yang, D. Peng, J. Lu, W. Yang, *J. Chem. Phys.* **2014**, *141*, 124104; b) F. Neese, *Coord. Chem. Rev.* **2009**, *253*, 526–563.

[15] P. Kubelka, F. Munk, *Z. Technol. Phys.* **1931**, *12*, 593–601.

[16] a) G. M. Sheldrick, *ShelXS97*, University of Göttingen, Germany, **1997**; b) G. M. Sheldrick, *ShelXL97*, University of Göttingen, Germany, **1997**.

[17] a) G. M. Sheldrick, XS. version 2013/1, University of Göttingen, Germany, **2013**; b) G. M. Sheldrick, *Acta Crystallogr., Sect. A* **2015**, *71*, 3–8; c) G. M. Sheldrick, *Acta Crystallogr., Sect. C Struct. Chem.* **2015**, *71*, 3–8.

[18] M. J. Frisch, G. W. Trucks, H. B. Schlegel, G. E. Scuseria, M. A. Robb, J. R. Cheeseman, J. A. Montgomery Jr., T. Vreven, K. N. Kudin, J. C. Burant, J. M. Millam, S. S. Iyengar, J. Tomasi, V. Barone, B. Mennucci, M. Cossi, G. Scalmani, N. Rega, G. A. Petersson, H. Nakatsuji, M. Hada, M. Ehara, K. Toyota, R. Fukuda, J. Hasegawa, M. Ishida, T. Nakajima, Y. Honda, O. Kitao, H. Nakai, M. Klene, X. Li, J. E. Knox, H. P. Hratchian, J. B. Cross, V. Bakken, C. Adamo, J. Jaramillo, R. Gomperts, R. E. Stratmann, O. Yazyev, A. J. Austin, R. Cammi, C. Pomelli, J. W. Ochterski, P. Y. Ayala, K. Morokuma, G. A. Voth, P. Salvador, J. J. Dannenberg, V. G. Zakrzewski, S. Dapprich, A. D. Daniels, M. C. Strain, O. Farkas, D. K. Malick, A. D. Rabuck, K. Raghavachari, J. B. Foresman, J. V. Ortiz, Q. Cui, A. G. Baboul, S. Clifford, J. Cioslowski, B. B. Stefanov, G. Liu, A. Liashenko, P. Piskorz, I. Komaromi, R. L. Martin, D. J. Fox, T. Keith, M. A. Al-Laham, C. Y. Peng, A. Nanayakkara, M. Challacombe, P. M. W. Gill, B. Johnson, W. Chen, M. W. Wong, C. Gonzalez, J. A. Pople, *Gaussian 03*, revision E.01, Gaussian, Inc., Wallingford, CT, **2004**.

[19] a) R. G. Parr, W. Yang, *Density Functional Theory of Atoms and Molecules*, Oxford University Press, Oxford, U. K., **1989**; b) D. R. Salahub, M. C. Zerner, *The Challenge of d and f Electrons*, ACS Symposium Series 394, American Chemical Society, Washington, DC, **1989**; c) W. Kohn, L. J. Sham, *Phys. Rev.* **1965**, *140*, A1133–A1138; d) P. Hohenberg, W. Kohn, *Phys. Rev.* **1964**, *136*, B864–B871.

[20] a) R. E. Stratmann, G. E. Scuseria, M. Frisch, *J. Chem. Phys.* **1998**, *109*, 8218–8224; b) M. E. Casida, C. Jamoroski, K. C. Casida, D. R. Salahub, *J. Chem. Phys.* **1998**, *108*, 4439–4449; c) R. Bauernschmitt, M. Haser, O. Treutler, R. Ahlrichs, *Chem. Phys. Lett.* **1996**, *256*, 454–464.

[21] a) A. D. Becke, *J. Chem. Phys.* **1993**, *98*, 5648–5652; b) B. Miehlich, A. Savin, H. Stoll, H. Preuss, *Chem. Phys. Lett.* **1989**, *157*, 200–206; c) C. Lee, W. Yang, R. G. Parr, *Phys. Rev. B* **1988**, *37*, 785–789.

[22] P. Pulay, *J. Comput. Chem.* **1982**, *3*, 556–560.

[23] H. B. Schlegel, J. J. McDouall, in: *Computational Advances in Organic Chemistry* (Eds.: C. Ogretir, I. G. Csizmadia), Kluwer Academic, The Netherlands, **1991**.

[24] a) P. J. Hay, W. R. Wadt, *J. Chem. Phys.* **1985**, *82*, 270–283; b) W. R. Wadt, P. J. Hay, *J. Chem. Phys.* **1985**, *82*, 284–298; c) P. J. Hay, W. R. Wadt, *J. Chem. Phys.* **1985**, *82*, 299–310.

[25] a) V. A. Rassolov, M. A. Ratner, J. A. Pople, P. C. Redfern, L. A. Curtiss, *J. Comput. Chem.* **2001**, *22*, 976–984; b) M. M. Francl, W. J. Pietro, W. J. Hehre, J. S. Binkley, D. J. DeFrees, J. A. Pople, M. S. Gordon, *J. Chem. Phys.* **1982**, *77*, 3654–3665; c) P. C. Hariharan, J. A. Pople, *Mol. Phys.* **1974**, *27*, 209–214; d) P. C. Hariharan, J. A. Pople, *Theo. Chim. Acta* **1973**, *28*, 213–

222; e) W. J. Hehre, R. Ditchfield, J. A. Pople, *J. Chem. Phys.* **1972**, *56*, 2257–2261.

[26] W. J. Hehre, R. Ditchfield, J. A. Pople, *J. Chem. Phys.* **1972**, *56*, 2257–2261.

[27] N. M. O'Boyle, A. L. Tenderholt, K. M. Langner, *J. Comput. Chem.* **2008**, *29*, 839–845.

[28] a) M. Cossi, N. Rega, G. Scalmani, V. Barone, *J. Comput. Chem.* **2003**, *24*, 669–681; b) V. Barone, M. Cossi, *J. Phys. Chem. A* **1998**, *102*, 1995–2001.

Received: May 5, 2016
Published Online: June 22, 2016

